Journal of Biomedical Optics

BiomedicalOptics.SPIEDigitalLibrary.org

Nanophotonic implementation of optoelectrowetting for microdroplet actuation

Christopher M. Collier
Kyle A. Hill
Mark A. DeWachter
Alexander M. Huizing
Jonathan F. Holzman

SPIE.

Nanophotonic implementation of optoelectrowetting for microdroplet actuation

Christopher M. Collier,* Kyle A. Hill, Mark A. DeWachter, Alexander M. Huizing, and Jonathan F. Holzman
The University of British Columbia, Integrated Optics Laboratory, 3333 University Way, Kelowna, British Columbia V1V 1V7, Canada

Abstract. The development and ultimate operation of a nanocomposite high-aspect-ratio photoinjection (HARP) device is presented in this work. The device makes use of a nanocomposite material as the optically active layer and the device achieves a large optical penetration depth with a high aspect ratio which provides a strong actuation force far away from the point of photoinjection. The nanocomposite material can be continuously illuminated and the position of the microdroplets can, therefore, be controlled to diffraction limited resolution. The nanocomposite HARP device shows great potential for future on-chip applications. [DOI: 10.1117/1.JBO.20.2.025004]

Keywords: biomedical optics; biophotonics; microfluidics; nanophotonics; ultrafast phenomena.

Paper 140813PR received Dec. 8, 2014; accepted for publication Jan. 16, 2015; published online Feb. 17, 2015.

1 Introduction

In recent years, great attention has been given to microfluidics technologies.[1–5] Microfluidics has many benefits for laboratory analyses, including increased portability, high throughput, low reagent volumes, and low power consumption, all of which come about from the microscale of the devices. Microfluidic devices can be found in many contemporary applications, including proteomics,[6] fluorescence imaging,[7] clinical diagnostics,[8] and DNA analysis.[9]

An intriguing subset of microfluidics that has emerged in recent years is digital microfluidics (DMF).[10–15] These DMF systems carry out two-dimensional (2-D) microdroplet actuation by way of perturbations to the on-chip electric field distribution. This allows DMF devices to be reconfigurable for a variety of analytical functions. Perturbations to the electric field distribution can come about from changes to the applied voltages on arrayed electrodes, as in standard electrowetting,[16,17] or even from light-induced changes to semiconductor conductivity on arrayed electrodes, as in optoelectrowetting.[18,19] This later technique has particular advantages for applications demanding small droplet size, precise microdroplet positioning, and minimal fabrication complexity.

For traditional optoelectrowetting, the DMF structure is activated by the optical triggering of an integrated photoconductive switch.[20] This attracts microdroplets to the illuminated position. Unfortunately, optoelectrowetting systems, similar to electrowetting systems, are discrete in nature and require on-chip integration of arrayed electrodes. The resolution for actuation is thus limited to the scale of the arrayed electrodes. To overcome the drawbacks due to the discrete nature of standard optoelectrowetting systems, Chiou et al.[21] introduced an innovative continuous optoelectrowetting (COEW) system that uses an amorphous-Si (a-Si) layer to provide microdroplet motion to any position above a single continuous electrode. The work presented here builds upon these findings.

In this work, COEW is demonstrated by way of optical activity in a nanocomposite layer having embedded semiconductor nanoparticles in a polymer host. The nanocomposite layer is implemented in a continuous plane to support COEW operation. The nanocomposite layer thickness is defined in accordance with the optical penetration depth of the illuminating beam. This leads to the formation of a localized "virtual electrode" with a high aspect ratio. It is found that the use of a nanocomposite layer and high-aspect-ratio photoinjection (HARP) allows for greater long-range horizontal forces compared to traditional a-Si photoinjection systems under the same illumination and bias electric field conditions. The material and structural considerations are presented for the implementation of such a nanocomposite HARP device.

2 Actuation Considerations

Actuation for the proposed COEW device is brought about by a continuous wave (cw) laser with an above-bandgap photon energy. The laser is focused from above onto the optically active layer to form a local "virtual electrode." Under such illumination, the semiconductor grains/particles form freely conducting charge-carriers, resulting in increased photoconductivity. The polarization of these charge-carriers from the applied voltage, V_b, leads to local space-charge screening which perturbs the electric field. The electric field perturbation attracts the microdroplet of interest to the illuminated focal spot.

In Figs. 1(a) and 1(b), respectively, cross sections of the representative traditional a-Si photoinjection device and new nanocomposite HARP device are shown. Each device has a continuous transparent indium tin oxide (ITO) top layer and a continuous copper bottom layer. These electrode layers are used to apply the bias voltage, V_b. Directly above the copper layer in Fig. 1(a) is a 10-μm thick a-Si layer, with a thickness that is approximately equal to its optical penetration depth. Directly above the copper layer in Fig. 1(b) is a 440-μm thick nanocomposite layer having Si or InP nanoparticles embedded in an insulative polydimethylsiloxane (PDMS) host. The PDMS is chosen because its high dielectric breakdown

*Address all correspondence to: Christopher M. Collier, E-mail: chris.collier@ubc.ca

1083-3668/2015/$25.00 © 2015 SPIE

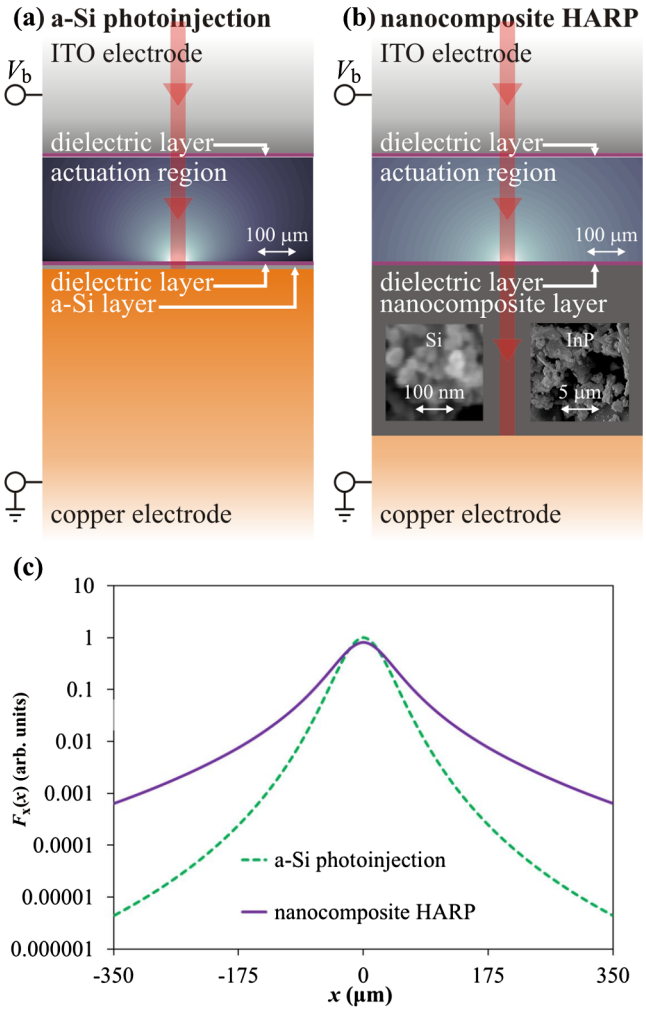

Fig. 1 Cross-sectional views of (a) the traditional a-Si photoinjection device and (b) the nanocomposite high-aspect-ratio photoinjection (HARP) device with embedded simulations. The simulations show the horizontal dielectrophoresis force in the actuation region as a grayscale map. (c) Representative cross section of the simulations at 40 μm of the way between the bottom electrode and top electrode. The results are shown as a normalized horizontal force, $F_x(x, y = 40\ \mu\text{m})$, as a function of the horizontal position, x, at the vertical position, $y = 40\ \mu$m. Note that $x = 0$ corresponds to the center of the illuminating beam.

strength, 2 MV/cm, supports the application of large bias electric fields and its high dielectric constant of 3.0 (Ref. 22) leads to increased polarizability. SEM images of the Si nanoparticles (with diameters down to 20 nm) and InP nanoparticles (with diameters down to hundreds of nanometers) are shown in Fig. 1(b) insets. The inner layers consist of two 10-μm thick dielectric layers made of polyethylene. In the 270-μm thick actuation region, an oil filler is used to surround the microdroplets of interest. With this configuration, the microdroplets have a contact angle of approximately 90 deg and this leads to decreased shear and contact line resistive forces (compared to those for an air filler).

In the traditional a-Si photoinjection device and nanocomposite HARP device, microdroplets undergo motion according to a horizontal dielectrophoresis force that is fundamentally based on the presence of a nonuniform electric field.[23] The nonuniform electric field produces a nonuniform polarization throughout the microdroplet—which leads to a nonuniform distribution of bound charge and a net actuation force for the microdroplet. The actuation regions of Figs. 1(a) and 1(b) show this horizontal dielectrophoresis force on a microdroplet that is present within a traditional a-Si photoinjection device and the proposed nanocomposite HARP device, respectively, for equal applied voltages. The results in these figures are generated by numerically integrating the contribution from charges on the electrodes to generate an electric field distribution, $E(x, y)$, as a function of the displayed horizontal (x) and vertical (y) dimensions. The electric field distribution seen in the x–y cross-sectional plane is used to compute the horizontal dielectrophoresis force, which is defined in proportion to the horizontal (x) component of $\nabla|E(x, y)|^2$. The actuation regions of Figs. 1(a) and 1(b) show the horizontal dielectrophoresis force as grayscale maps, with white indicating increased magnitude, for the traditional a-Si photoinjection device and proposed nanocomposite HARP device, respectively. It is seen that the proposed nanocomposite HARP device produces actuation over a longer range compared to that of the traditional a-Si photoinjection device. This distinction for the ranges is quantified in Fig. 1(c), which plots the normalized horizontal dielectrophoresis force, $F_x(x, y = 40\ \mu\text{m})$, for the a-Si photoinjection device (green dashed line) and nanocomposite HARP device (purple solid line) as a function of the horizontal, x, dimension at $y = 40\ \mu$m. For the nanocomposite HARP device, the long-range electric field gradients result from photoinjection with an accentuated vertical dimension, i.e., high aspect ratio. For the traditional device, photoinjection is carried out with a flatter profile, i.e., low aspect ratio, and this yields electric field lines that mimic a parallel plate capacitor—with largely vertical electric field lines and minimal fringing fields (that would be needed to induce long-range microdroplet actuation). It should be noted that the large penetration depths required for nanocomposite HARP devices, being on the order of hundreds of microns, cannot be achieved with existing crystalline, polycrystalline, or amorphous semiconductors.

The nanocomposite HARP device relies on optical activity to actuate droplets. Therefore, it is important that the semiconductor nanoparticles undergo charge-carrier photogeneration and subsequent recombination upon photoexcitation. To investigate the charge-carrier dynamics of the Si nanoparticles, pump–probe experiments are performed. These experiments use an ultrafast pulsed laser to pump the material at a 780-nm wavelength yielding photogenerated charge-carriers and probe at a 1550-nm wavelength to sample the time-varying charge-carrier density. A pump-probe scan of the Si nanoparticles is shown in Fig. 2 as a solid red line. It is seen that the Si nanoparticles undergo charge-carrier photogeneration and rapid recombination in a duration less than 10 ps. This short lifetime results from the dominance of charge-carrier diffusion and surface recombination within the nanoparticles—as the nanoparticle diameter is much less than the charge-carrier diffusion length and this leads to an increased contribution from surface recombination states.[24] A pump-probe scan of the Si crystalline material, shown in Fig. 2 as a dashed red line, exhibits a much longer recombination time in comparison to that of the Si nanoparticles. Pump-probe scans of the Si nanoparticles are also carried out with applied bias voltages (not shown), and it is found that charge-carrier drift resulting from the applied bias fields has little contribution to the observed optical activity. The relatively low signal levels seen here for the Si nanoparticle

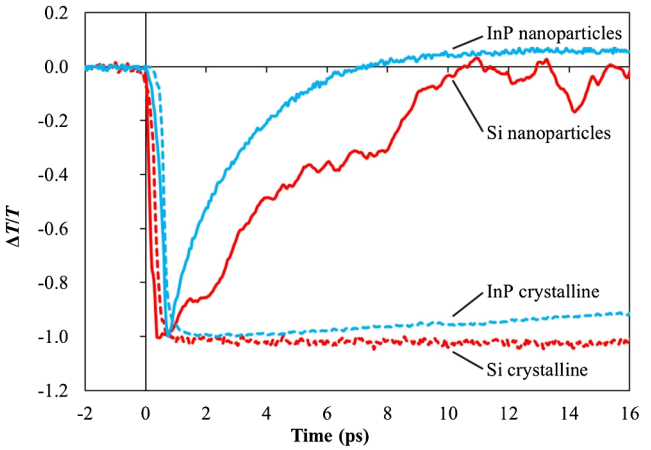

Fig. 2 Experimental pump-probe results are shown for Si crystalline material, Si nanoparticles, InP crystalline material, and InP nanoparticles.

and crystalline materials are a result of the indirect bandgap of Si. These considerations on optoelectronic conversion efficiency are addressed in the following section.

It is worth noting that the proposed nanocomposite HARP device benefits from enhanced control of diffusion in the nanocomposite material compared to devices based on crystalline, polycrystalline, or amorphous semiconductors. In terms of charge-carrier diffusion, the nanocomposite material yields negligible migration of electrons and holes between neighboring nanoparticles through the PDMS host. Thus, the illuminating beam can accurately define the region of optical activity, i.e., it can accurately define the size and location of the "virtual electrode" that is applied for microdroplet actuation. In terms of thermal diffusion, the nanocomposite material can localize heating in regions that are distant from the actuated microdroplet and thereby minimize the effects of evaporation. This comes about from (i) the small thermal diffusivity of the nanocomposite material which has restricted heat diffusion through the insulative PDMS host, and (ii) the long-range actuation force that can be induced by the nanocomposite HARP device which allows the illuminating beam to be applied far from the microdroplet of interest. The control of thermal diffusion is particularly important given the potential for a large difference between the illuminating beam photon energy and the semiconductor bandgap, which can lead to significant excess energy dissipation through phonon emission. These considerations on thermal diffusion are addressed in the following section.

A SolidWorks schematic of the full experimental setup of the nanocomposite HARP device is shown in Fig. 3. A focused 650 nm cw laser beam is directed onto the nanocomposite HARP device through an adjustable mirror that allows for full 2-D illumination of the nanocomposite HARP device. To record the microdroplet motion in the experiment, an observation mirror and imaging camera are used.

3 Device Operation

The proof-of-principle operation of the nanocomposite HARP device with Si nanoparticles is shown in the results of Fig. 4. In this nominal experiment, the nanocomposite HARP device is operated with a deionized water microdroplet that is 500 μm in diameter and 53 nL in volume. The applied DC voltage is $V_b = 2.5$ kV. The nanocomposite HARP device is

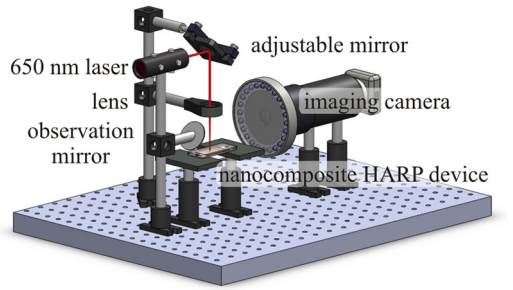

Fig. 3 SolidWorks schematic of the complete experimental setup for the nanocomposite HARP device.

illuminated by a cw 650-nm laser having 5 mW of power with a spot size diameter of approximately 200 μm. In the initial position of Fig. 4(a), the microdroplet is unilluminated. The focused laser beam is then applied to a spot 460 μm away from the initial microdroplet position. This illumination makes the microdroplet move toward the illuminated spot and the microdroplet ultimately comes to rest at the illuminated position. This motion can be seen as a transition to the final state of the microdroplet seen in Fig. 4(b).

A more intricate merging process is also performed and the results from this experiment are shown in Fig. 5. In this nominal experiment, the nanocomposite HARP device with Si nanoparticles is operated with two deionized water microdroplets that are 900 μm in diameter and 170 nL in volume. The applied DC voltage is $V_b = 1$ kV. The nanocomposite HARP device is illuminated by the same 650 nm, 5 mW focused cw laser beam. In the initial position of Fig. 5(a), both microdroplets are unilluminated and there is an initial 2460 μm horizontal distance between the microdroplets. The focused laser beam is then applied to cause the left microdroplet to be actuated toward the right microdroplet. An intermediate position for the motion is shown in Fig. 5(b). Here, the left microdroplet has begun its motion toward the right microdroplet and the microdroplets are positioned with 1620 μm horizontal spacing between them. A second intermediate position is shown in Fig. 5(c) where the microdroplets now have only a 1230 μm horizontal separation between them. The final state is shown in Fig. 5(d) with the microdroplets having been merged. The merged microdroplet has a diameter of 1260 μm and a volume of 340 nL, and it has settled into a stable state with a circular profile. The device operates with microdroplet speeds up to approximately 50 μm/s.

To refine the operation of the nanocomposite HARP device, it is necessary to address the poor optoelectronic conversion efficiency of the Si nanoparticles. The optoelectronic response

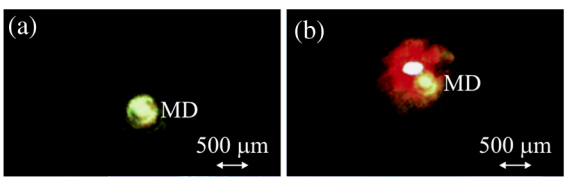

Fig. 4 The experimental operation of the Si-based nanocomposite HARP device is shown. The device is operated with a 500-μm diameter microdroplet of 53 nL volume with 650 nm continuous wave (cw) laser illumination. The microdroplet, labeled as MD, is actuated a distance of 460 μm from (a) the initial position (unilluminated) to (b) the final position (illuminated).

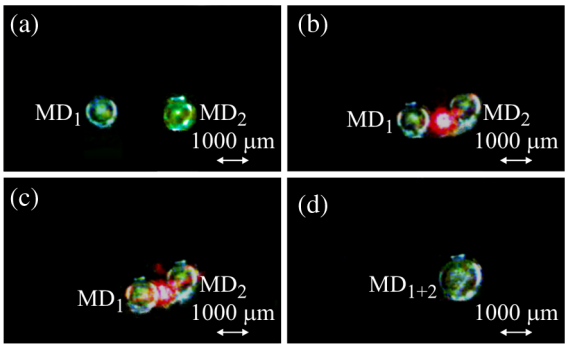

Fig. 5 The experimental operation of the Si-based nanocomposite HARP device is shown for a merging process. The device is operated with two 900-μm diameter microdroplets of 170 nL volume with 650 nm cw laser illumination. The following chronological images are shown: (a) the initial positions of the two microdroplets, labeled MD_1 and MD_2, (b) an early intermediate state, (c) a later intermediate stage, and (d) the final merged microdroplet, labeled MD_{1+2}. The final microdroplet has a 1260-μm diameter and 340-nL volume.

of Si, an indirect bandgap semiconductor, has a low optoelectronic conversion efficiency because phonon-assisted transitions are needed to create electron-hole pairs. In contrast, the optoelectronic response of InP, being a direct bandgap semiconductor, facilitates a nearly 100% optoelectronic conversion efficiency of photons to electron-hole pairs. The dissimilar optoelectronic conversion efficiencies of InP and Si are seen by way of the data presented in Fig. 2, which includes pump-probe scans for the InP nanoparticle (shown as the solid blue line) and crystalline (shown as the dashed blue line) materials. The data of Fig. 2 show an increased carrier density and improved signal level for InP over that of Si by approximately 2.5 times. The benefits of InP are also seen in terms of decreased thermal energy dissipation. When InP (with a 1.3 eV bandgap) and Si (with a 1.1 eV bandgap) are illuminated with 650 nm photons having a 2.0 eV photon energy, the photogenerated electrons in InP have a lower excess energy, which is $2.0 - 1.3\ \text{eV} = 0.7\ \text{eV}$, than that of Si, which is $2.0 - 1.1\ \text{eV} = 0.9\ \text{eV}$. This leads to a decrease in wasted thermal energy due to phonon emission. For the 200 μm illumination spot size used with the Si and InP systems, the applied (optical) power per unit area of 160 mW/mm^2 leads to dissipated (heat) powers per unit area of approximately 72 and 56 mW/mm^2, respectively. (If necessary, such heating can be made negligible by matching the photon energy of the illuminating beam to the bandgap energy of the semiconductor in the nanocomposite).

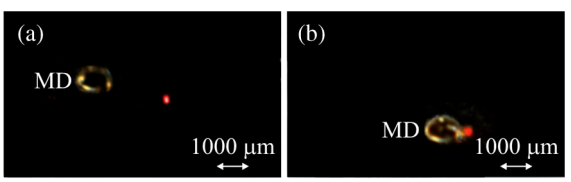

Fig. 6 The experimental operation of the InP-based nanocomposite HARP device is shown for actuation of biological fluid. The device is operated with one 1100-μm diameter and 260-nL volume microdroplet, having 25% concentration of egg albumin, labeled MD, with 650 nm cw laser illumination. The microdroplet is actuated a distance of 1700 μm from (a) the initial position (unilluminated) to (b) the final position (illuminated).

With the advantages of InP in mind, the nanocomposite HARP device is modified to use InP nanoparticles instead of Si nanoparticles. With a nanocomposite HARP device based on InP nanoparticles, the device can be optimized for operation with microdroplets containing biological fluids, which are typically less polarizable and more difficult to actuate compared to deionized water microdroplets. The material for the semiconductor nanoparticles is selected to be InP as it gives an increased optoelectronic conversion efficiency, and the volumetric ratio of the nanoparticle-polymer ratio of the nanocomposite material is selected to tune/increase the optical penetration depth to the desired high-aspect-ratio profile. Note that such a tunability for the optical penetration depth is not facilitated by standard semiconductor thin-film deposition techniques.

Operation of the nanocomposite HARP device with InP nanoparticles is shown in the experimental results of Fig. 6. In this experiment, the device is operated with a microdroplet of 25% concentration egg albumin protein. The microdroplet size, 1100 μm in diameter and 260 nL in volume, is comparable to that used with the Si nanocomposite HARP device. The nanocomposite HARP device is illuminated by a 650 nm, 5 mW cw laser beam. An AC voltage of $V_b = 610\,V_{rms}$ is used in this experiment with an optimal actuation frequency of 470 Hz to facilitate easier microdroplet actuation with the biological protein. (Experimental[25] and theoretical[26] analyses for the optimal AC actuation frequencies are shown elsewhere.) In the initial position of Fig. 6(a), the microdroplet is unilluminated. The focused laser beam is then applied to a spot that is 2640 μm away from the microdroplet's initial position. This illumination makes the microdroplet move toward the illuminated spot at a speed of up to approximately 100 $\mu\text{m}/\text{s}$, and the microdroplet ultimately comes to rest in the illuminated position. This motion can be seen as a transition to the final microdroplet position in Fig. 6(b).

4 Conclusion

The development and ultimate operation of a nanocomposite HARP device was presented in this work. By making use of a nanocomposite material as the optically active layer, the device achieved a large optical penetration depth with a high aspect ratio which provided strong actuation forces far away from the point of photoinjection. As the nanocomposite material can be continuously illuminated, the position of the microdroplets can be controlled to diffraction limited resolution. The nanocomposite HARP device showed great potential for future on-chip applications.

Acknowledgments

This work was supported by the Natural Sciences and Engineering Research Council of Canada (NSERC), Canadian Foundation for Innovation, and Western Economic Diversification. The authors would like to thank D.J. Arkinstall for SEM technical expertise.

References

1. M. Li et al., "Microfluidic surface-enhanced Raman scattering sensor with monolithically integrated nanoporous gold disk arrays for rapid and label-free biomolecular detection," *J. Biomed. Opt.* **19**(11), 111611 (2014).
2. J.-H. Lee and J.-K. Song, "Degradation of electrowetting for upward and downward electrolyte droplets containing microparticles," *Appl. Phys. Lett.* **104**, 081610 (2014).

3. J. Wu and M. Gu, "Microfluidic sensing: state of the art fabrication and detection techniques," *J. Biomed. Opt.* **16**(8), 080901 (2011).
4. N. M. M. Pires et al., "Integrated optical microfluidic biosensor using a polycarbazole photodetector for point-of-care detection of hormonal compounds," *J. Biomed. Opt.* **18**(9), 097001 (2013).
5. V. Horowitz, D. Awschalom, and S. Pennathur, "Optofluidics: field or technique?," *Lab Chip* **8**, 1856–1863 (2008).
6. J. Lee, S. A. Soper, and K. K. Murray "Microfluidics with MALDI analysis for proteomics—a review," *Anal. Chim. Acta* **649**, 180–190 (2009).
7. A. Shanmugam and C. Salthouse, "Lensless fluorescence imaging with height calculation," *J. Biomed. Opt.* **19**(1), 016002 (2014).
8. T. Li et al., "Out-of-plane microvalves for whole blood separation on lab-on-a-CD," *J. Micromech. Microeng.* **20**, 105024 (2010).
9. T. Humphreys et al., "World-to-chip interconnects for efficient loading of genomic DNA into microfluidic channels," *J. Micromech. Microeng.* **19**, 105024 (2009).
10. M. H. Shamsi et al., "A digital microfluidic electrochemical immunoassay," *Lab Chip* **14**, 547–554 (2014).
11. K. Chakrabarty, R. B. Fair, and J. Zeng, "Design tools for digital microfluidic biochips: toward functional diversification and more than moore," *IEEE Trans. Comput.-Aided Design Integr. Circuits Syst.* **29**, 1001–1017 (2010).
12. M. Abdelgawad and A. R. Wheeler, "Low-cost, rapid-prototyping of digital microfluidics devices," *Microfluid. Nanofluid.* **4**, 349–355 (2008).
13. J. Nichols et al., "On-chip digital microfluidic architectures for enhanced actuation and sensing," *J. Biomed. Opt.* **17**(6), 067005 (2012).
14. S. L. S. Freire and B. Tanner, "Additive-free digital microfluidics," *Langmuir* **29**, 9024–9030 (2013).
15. T. Lederer et al., "Integration of impedance spectroscopy sensors in a digital microfluidic platform," *Microsyst. Technol.* **18**, 1163–1180 (2012).
16. I. A. Eydelnant, B. B. Li, and A. R. Wheeler, "Microgels on-demand," *Nat. Commun.* **5**, 3355 (2014).
17. C. M. Collier et al., "Nonlinear dual-phase multiplexing in digital microfluidic architectures," *Micromachines* **2**(4), 369–384 (2011).
18. P.-Y. Chiou, Z. Chang, and M. C. Wu, "Droplet manipulation with light on optoelectrowetting device," *J. MEMS* **17**(1), 133–138 (2008).
19. S.-Y. Park and P.-Y. Chiou, "Light-driven droplet manipulation technologies for lab-on-a-chip applications," *Adv. Optoelectron.* **2011**, 909174 (2011).
20. D. H. Auston, "Picosecond optoelectronic switching and gating in silicon," *Appl. Phys. Lett.* **26**, 101–103 (1975).
21. P. Y. Chiou, S.-Y. Park, and M. C. Wu, "Continuous optoelectrowetting for picoliter droplet manipulation," *Appl. Phys. Lett.* **93**, 221110 (2008).
22. S. C. B. Mannsfeld et al., "Highly sensitive flexible pressure sensors with microstructured rubber dielectric layers," *Nat. Mater.* **9**, 859–864 (2010).
23. C. M. Collier, K. A. Hill, and J. F. Holzman, "A dielectrophoresis microjet for on-chip technologies," *RSC Adv.* **3**(45), 23309–23316 (2013).
24. C. M. Collier and J. F. Holzman, "Ultrafast photoconductivity of crystalline, polycrystalline, and nanocomposite ZnSe material systems for terahertz applications," *Appl. Phys. Lett.* **104**(4), 042101 (2014).
25. R. B. Fair, "Digital microfluidics: is a true lab-on-a-chip possible?," *Microfluid. Nanofluid.* **3**, 245–281 (2007).
26. F. Krogmann et al., "Push/pull actuation using opto-electrowetting," *Sens. Actuator A* **141**, 499–505 (2008).

Christopher M. Collier received the BASc. degree in electrical engineering from the University of British Columbia, Kelowna, BC, Canada, in 2011, where he is currently pursuing the PhD degree in electrical engineering.

Kyle A. Hill is currently enrolled in the BASc. degree in electrical engineering at the University of British Columbia, Kelowna, BC, Canada.

Mark A. DeWachter is currently enrolled in the BASc. degree in mechanical engineering at the University of British Columbia, Kelowna, BC, Canada.

Alexander M. Huizing is currently enrolled in the BASc. degree in mechanical engineering at the University of British Columbia, Kelowna, BC, Canada.

Jonathan F. Holzman received the BSc. degree in engineering physics and the PhD degree in electrical engineering from the University of Alberta, Edmonton, AB, Canada, in 1998 and 2003, respectively. He was a Postdoctoral research fellow with the Department of Information Technology and Electrical Engineering, Swiss Federal Institute of Technology, Zürich, Switzerland, from 2004 to 2005. He is currently an associate professor with the School of Engineering, University of British Columbia, Kelowna, BC, Canada.